NINTH EUROPEAN ROTORCRAFT FORUM

Paper No. 60

STRUCTURAL AND DYNAMIC TAILORING OF HINGELESS/BEARINGLESS ROTORS

G. Seitz
G. Singer

MESSERSCHMITT-BÖLKOW-BLOHM GMBH
MUNICH, GERMANY

September 13-15, 1983
STRESA, ITALY

Associazione Industrie Aerospaziali
Associazione Italiana di Aeronautica ed Astronautica

STRUCTURAL AND DYNAMIC TAILORING OF HINGELESS/BEARINGLESS ROTORS

G. Seitz
G. Singer

Messerschmitt-Bölkow-Blohm GmbH
Munich, Germany

Abstract

This paper presents a realization of a concept for bearingless main and tail rotors by using special fibreglass flexural torsion-bending elements. The dynamic and structural requirements concerning the torsional stiffness as well as the stiffness inplane and out-of-plane of the rotor are discussed in detail. Special analytical and experimental activities were carried out for the development of flexible elements, blade lead-lag elastomeric dampers, hub design with composite materials, pitch control system and blade attachment.

Theoretical solutions and test results for a four-bladed main and tail rotor are reported and critically compared.

1. Introduction

In the past, considerable efforts have been carried out by helicopter manufacturers and research organizations in the development of advanced main rotors. The introduction of new composite materials for the blades and the rotor hub offered the chance to realize these modern rotor concepts.

During the last two decades, the hingeless rotor system and, more recently, the bearingless rotor concept have found continuously growing interest. The reason for the development of the bearingless rotor concept is its simplicity, which improves the reliability and maintainability of the rotor and which potentially reduces the weight, drag and costs of the system as well. In the following table there are summarized the various activities of the helicopter industry concerning bearingless main and tail rotors. More details may be found in Ref. 1 for instance.

This paper presents the four-bladed bearingless main and tail rotor systems, presently developed at MBB. Figure 1 shows the experimental versions of both rotors. These rotors will be flight tested on MBB's light utility class helicopters in the very near future. Interesting rotor data are summarized in the appendix for convenience.

COMPANY	MAIN-ROTORS		TAIL-ROTORS	
	in Production	Experimental	in Production	Experimental
BOEING VERTOL		BMR Experimental Rotor on BO 105		UTTAS Flex Strap
BELL		Model 680		Experimental see-saw *)
HUGHES				Composite Flexbeam
KAMAN				(Elastic pitch beam TR)
SIKORSKY			Black HAWK S70 S76	
SNIAS AEROSPATIALE		Triflex	AS 355 *) see-saw	Triflex
MBB		Composite Flex-Beam		Composite Flex-Beam

*) with elastomeric flap bearing

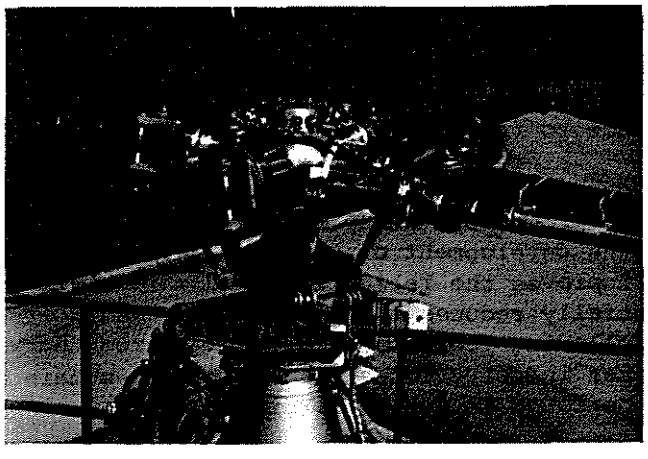

Main Rotor

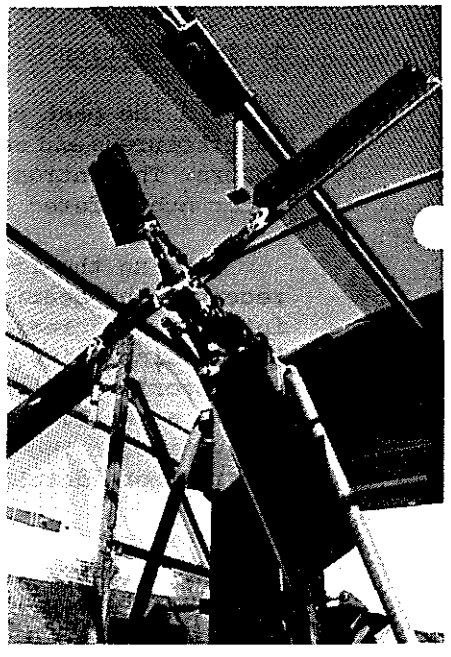

Tail Rotor

Figure 1 The Experimental Main Rotor and Tail Rotor

In the past, positive experience with the soft-inplane rotor concept has been gained at MBB. Therefore both the bearingless main and tail rotor are designed as soft-inplane configurations. It is well known that the cantilever attachment of the blades to the hub increases the control power and damping capacity of the rotor.

Relative to current hingeless rotor systems there is a trend to reduce the hub flap moment stiffness for advanced bearingless rotor configurations. A reduced flap stiffness lowers gust and vibration sensitivity and minimizes adverse flight mechanical effects at high speeds. In addition, special lead-lag damping devices must be provided for the bearingless rotor configuration in order to improve the aeromechanical stability. Regarding the structural strength of the composite materials used in the bearingless rotor, attention must be paid to the integration of these goals into the overall design requirements of the rotor system. More details about MBB's bearingless rotor concept will be given in the following sections; see also Ref. 2 and 3.

2. The Torsional Part of the Flexbeam Element

In the bearingless rotor concept, the mechanical pitch bearings are replaced with a flexbeam. Therefore the design of the torsional elastic part of the flexbeam is of central importance. It has to meet the following requirements:

- Blade feathering should be possible by small control forces.
- High pitch angles must be possible.
- High torsional deformation should be restricted to a well-defined flexbeam element, which should be as short as possible.
- As a part of the blade structure, a complex loading has to be carried by the torsional elastic element.

Therefore the designer has to combine a short active length of the element with a low torsional stiffness. This minimization is limited by the ultimate shear stresses.

There are several possiblities of cross-sections of the torsional-elastic-elements which satisfy these requirements. Special investigations show that elements with T and cruciform cross-sections are favourable for the rotor design. Figure 2 shows the two cross-sections which are used for the main rotors.

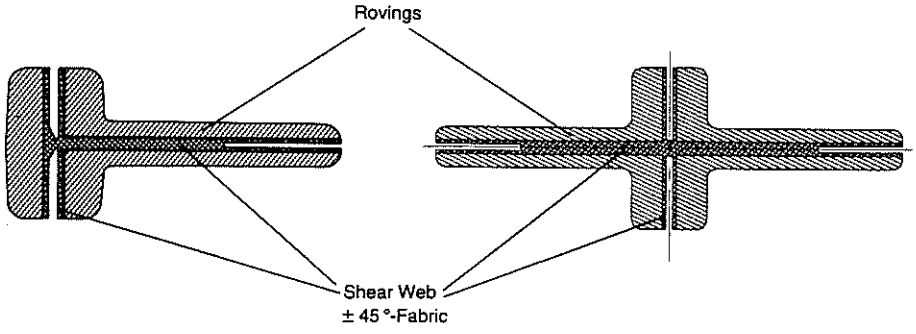

Figure 2 Cross-Section of Two Torsional Elastic Elements (Main Rotor)

Both cross-sections have the same typical composition. Near the axis of symmetry or the tension axis (neutral axis of bending) respectively there is the shear web, which is built up of $\pm$ 45° GFRP-fabric. This inner core of the cross-section, which is shown in Figure 3 for the tail rotor flex-beam element, has to carry the shear forces due to the twisting

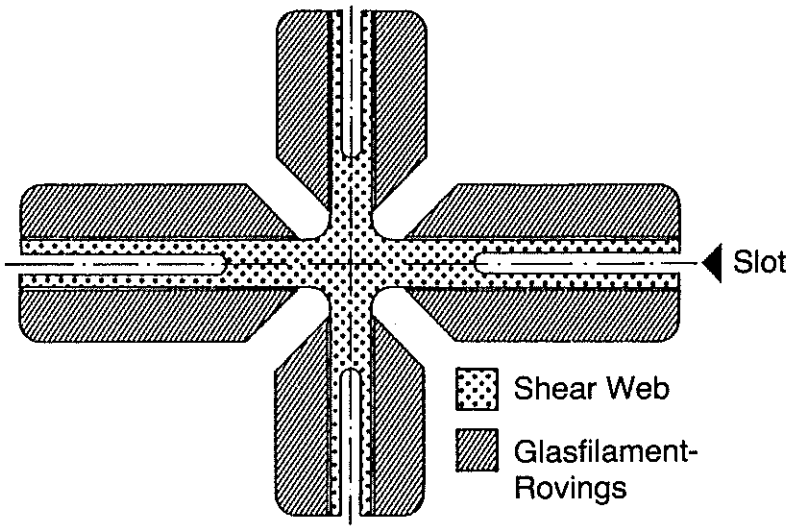

Figure 3 Cross-Section of Flexbeam Element Without Damper (Tail Rotor)

moments as well as the transverse forces in flapwise and chordwise directions. As the torsional stiffness is strongly dependent on the thickness, the shear web is slotted to reduce the torsional stiffness. Unidirectional glass filament rovings are stuck on the webs in order to carry the centrifugal load and to obtain the desired bending stiffness in flapping and lead-lag directions. As the rovings have a high longitudinal stiffness and a small shear stiffness, it is an advantage to place them at a certain distance from the neutral axis, thus increasing the bending stiffness, while the influence on the shear stiffness is of lower order. A finite element model was used to investigate the torsional elastic element, which is mainly loaded by shear stresses, owing to the maximum pitch angle (Ref. 4). The idealized cross-section for the tail rotor with damper is shown in Figure 4.

These constructions have the following advantages:

- Low torsional stiffness can be realized by these cross-sections.

- Because of the physical characteristics of star-like profiles, the considered cross-sections induce no secondary shear stresses owing to warping.

- The required stiffnesses in flapwise and chordwise directions can be designed independent of each other by varying the geometrical data of the roving packages. In the same way, there is nearly no superposition of the stresses due to the flapwise bending and the chordwise bending.

- The cross-type elements have no product of inertia.

- The center of mass, the elastic center and the shear center coincide, so that no torsional moments due to bending occur.

- The restoring torsional moment owing to the centrifugal force can be kept small, thus there is no great difference between the torsional stiffness with and without centrifugal load.

- The application of integrated elastomeric lead-lag dampers is possible near the virtual lead-lag hinge and they are virtually uninfluenced by the flapping motion. Figure 5 shows the location of the dampers for the experimental main rotor.

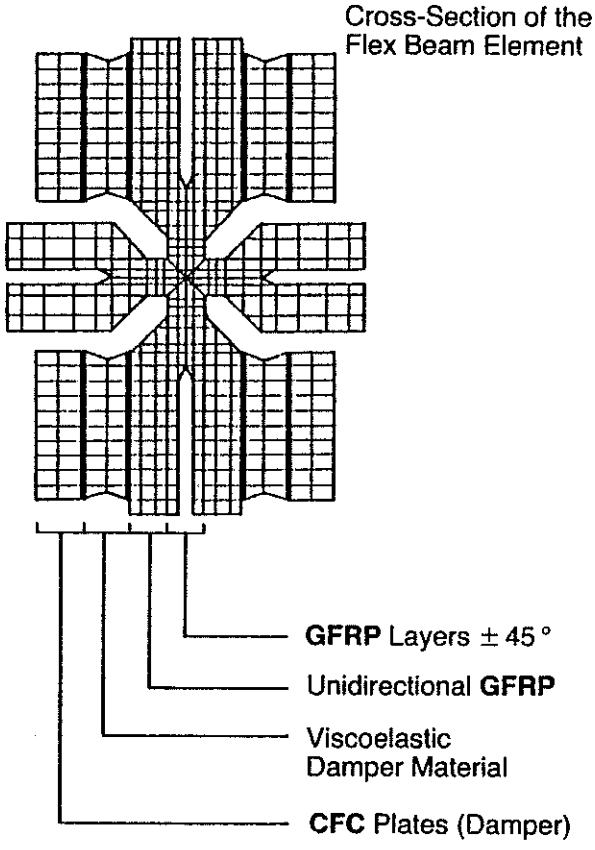

Figure 4 Flexbeam Cross-Section Idealization With Damper (Tail Rotor) FEM Stress Calculation

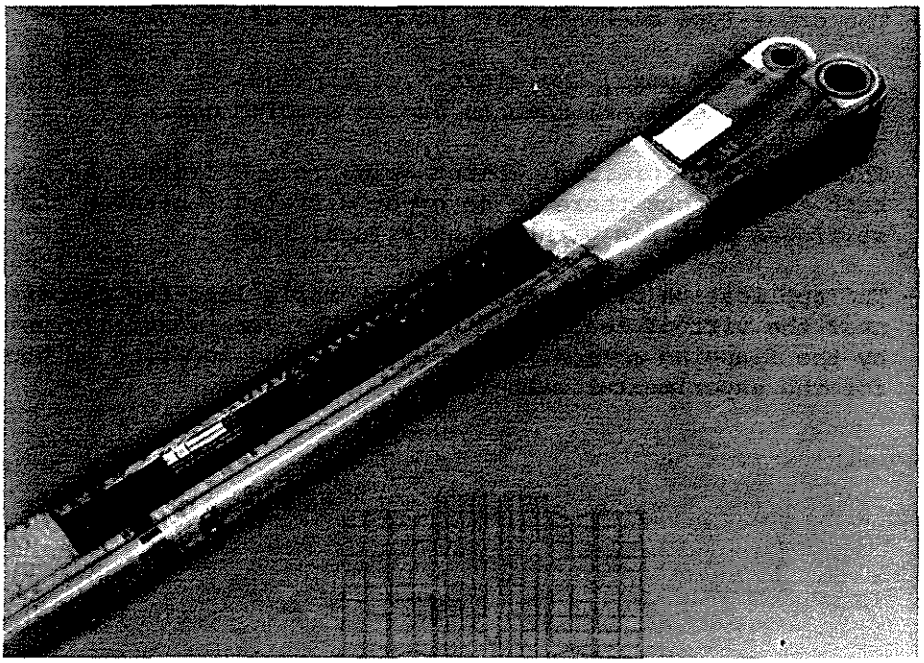

Figure 5 Blade Root and Flexbeam With Damper of the Experimental Main Rotor

3. Development of the Bearingless Main Rotor

The development of a bearingless main rotor has been based on the hingeless BO 105 system with an experimental rotor as a intermediate step, see Figure 6. The experimental rotor does not yet satisfy the final

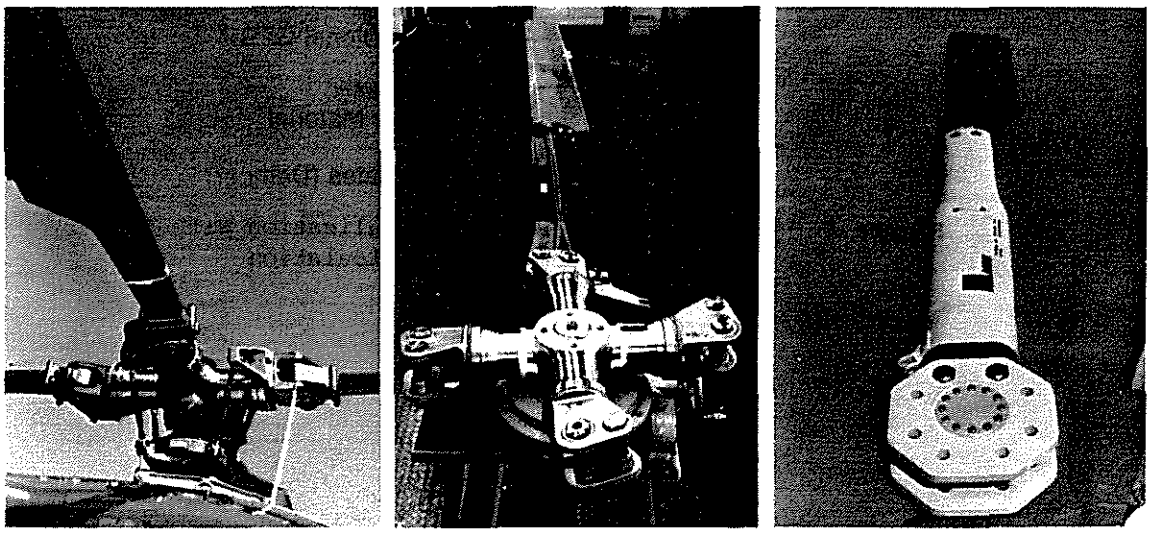

Figure 6 The Development from the Hingeless BO105 Rotor Concept to the Bearingless Rotor Concept

system requirements. The aim of this program was to realize a bearingless system in a short time, in order to obtain some experience from component, whirl-tower and flight tests. Meanwhile, the component tests and the whirl-tower experiments were performed successfully, the flight tests are scheduled for the autumn of this year. The final rotor concept is presently being developed (see Ref. 5). Whirl-tower tests will be carried out during the next year.

3.1 Experimental Bearingless Rotor Concept

Description of the Experimental Rotor

The rotor hub of the experimental rotor is a BO 105 production hub with a fixed pitch motion in the middle, see Fig. 6. The blade attachment is made with two bolts. The torsional elastic element has a T-form cross-section, see also Fig. 2, left. The inboard end of the flexbeam is attached directly to the hub, whereas the outboard end of the flexbeam is attached to the outer part of the blade. The control rod attaches to the junction of the flexbeam and the blade. The blade for the experimental rotor is the same as the production blade of the BO 105 rotor.

The pitch of the blade is controlled by a stiff rod of $\pm 45^{\circ}$ CFC, which is connected to the pitch horn and the rotor blade by two elastic couplings. Therefore the control rod is primarily loaded by torsional moments. In order to augment the lead-lag blade damping, an elastomeric damper has been developed, see Fig. 5. More details of the working principle are given later. In addition, the lead-lag damping is further improved by introducing pitch-lead coupling. A preflap angle of 2.0° has been built in at the junction of the blade. For the same reason the precone angle has been reduced from 2.5° to 1.0°.

Blade Stiffness Distribution

The bending stiffnesses in flapwise and chordwise directions of the experimental rotor are shown in Figure 7 and are compared with the BO 105 stiffness values.

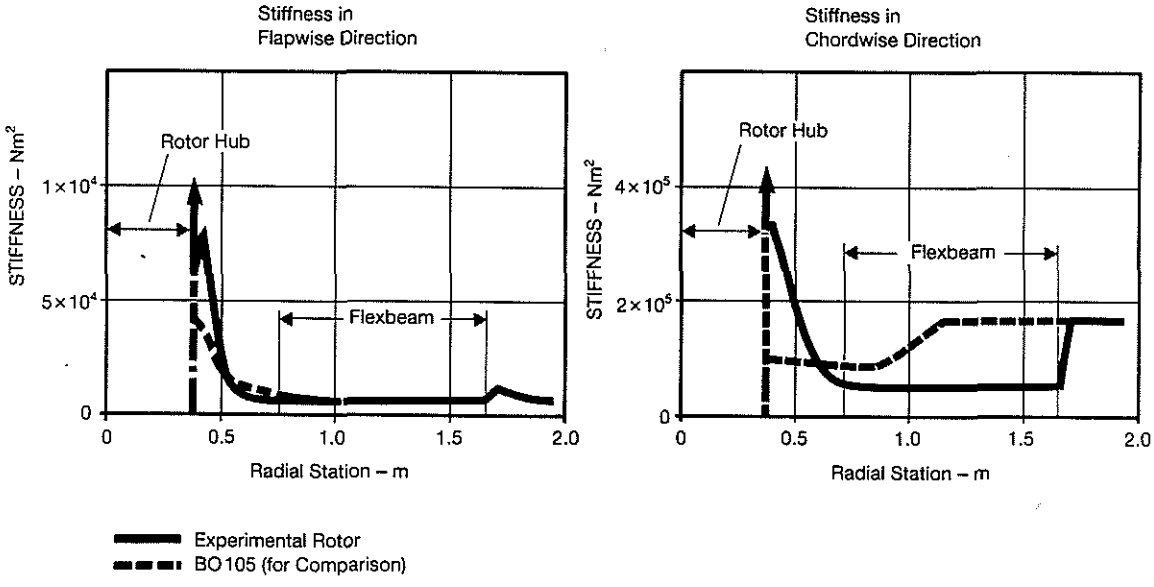

Figure 7 Bending Stiffness - Comparison Between Experimental Rotor and BO105

Blade Natural Frequencies

The experimental bearingless rotor is designed to fly on the BO 105 helicopter and has flap, chord and torsion frequencies at approximately the current BO 105 values. The uncoupled blade natural bending frequencies of both rotor systems are plotted versus rotor speed in Figure 8.

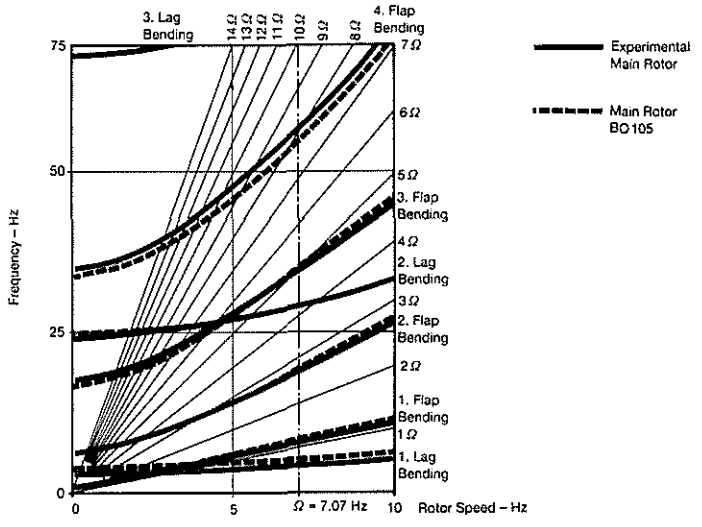

Figure 8 Main Rotor Blade Natural Frequencies - Comparison Between Experimental Rotor and BO105 Rotor Blade

Laboratory Tests

The blade root and flexbeam elements were fatigue tested in the bending machine, see Figure 9. The applied forces and the corresponding load cycles are summarized in the following table.

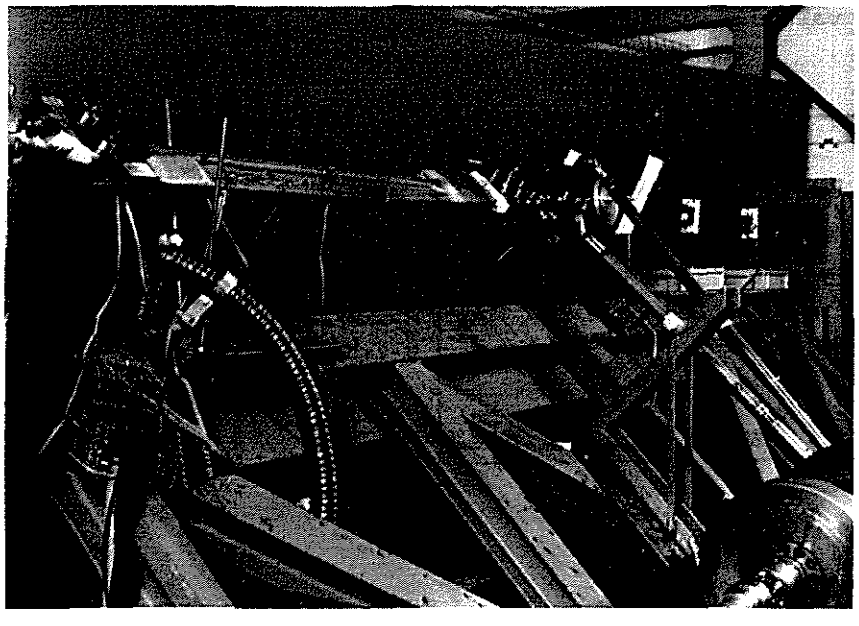

Figure 9 Laboratory Test Setup of the Experimental Main Rotor

Load Cycles	Root Bending Moments		Pitch Angle
	M_β [Nm]	M_ζ [Nm]	
$0 \div 1.7 \cdot 10^6$	1480 ± 910	1500 ± 2230	$3^o \pm 9^o$
$1.7 \cdot 10^6 \div 3.9 \cdot 10^6$	1160 ± 1420	1250 ± 2200	$5^o \pm 9^o$
$3.9 \cdot 10^6 \div 8 \cdot 10^6$	1060 ± 1580	1260 ± 2400	$5^o \pm 12^o$

These high loads represent relatively rare flight manoeuvres, therefore the number of load cycles correspond to a life time of about 10 000 flight hours on the BO 105 helicopter. Of special interest was the torsional stiffness of the flexbeam element reaching values of 6 Nm/^{o} without tension and 8 Nm/^{o} with tension respectively.

Whirl Tower Test

After the successful component tests, the experimental rotor was installed on the whirl tower, see Fig. 1 left. The following items should be proved and tested in detail:

- Natural frequencies at zero and nominal rotor speed.
- Effectiveness of the elastomeric dampers.
- Stresses and strains at critical stations of the rotor system for different control angles.
- Endurance test.

Some test results are now summarized. The measured and calculated natural frequencies are compared in the frequency diagram of Figure 10.

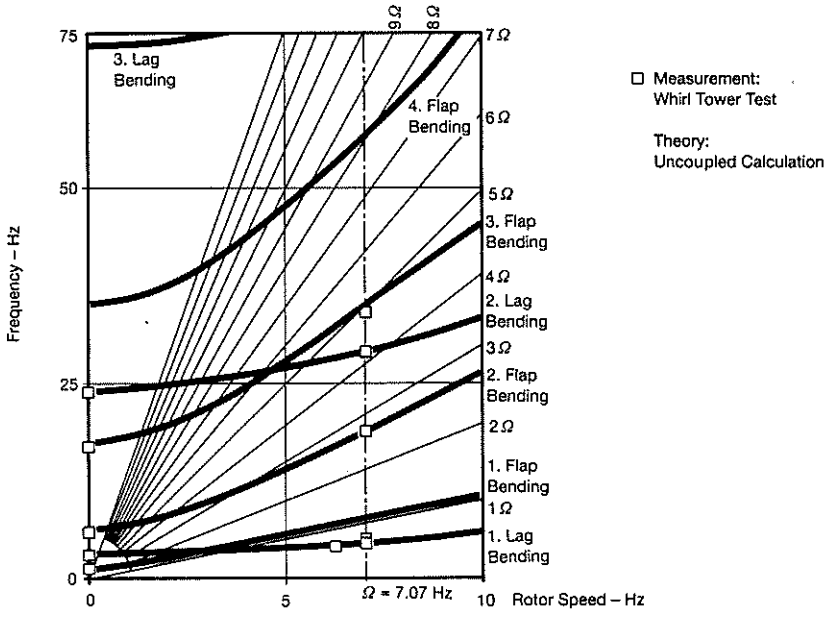

Figure 10 Experimental Main Rotor Blade Natural Frequencies - Theory and Measurement

The mechanics of the newly developed elastomeric blade damper system and the lead-lag damping of the fundamental mode at different pitch settings are shown in Figure 11. The damper consists of a viscoelastic layer which is attached to the flexbeam and covered by a stiff carbon fibre beam.

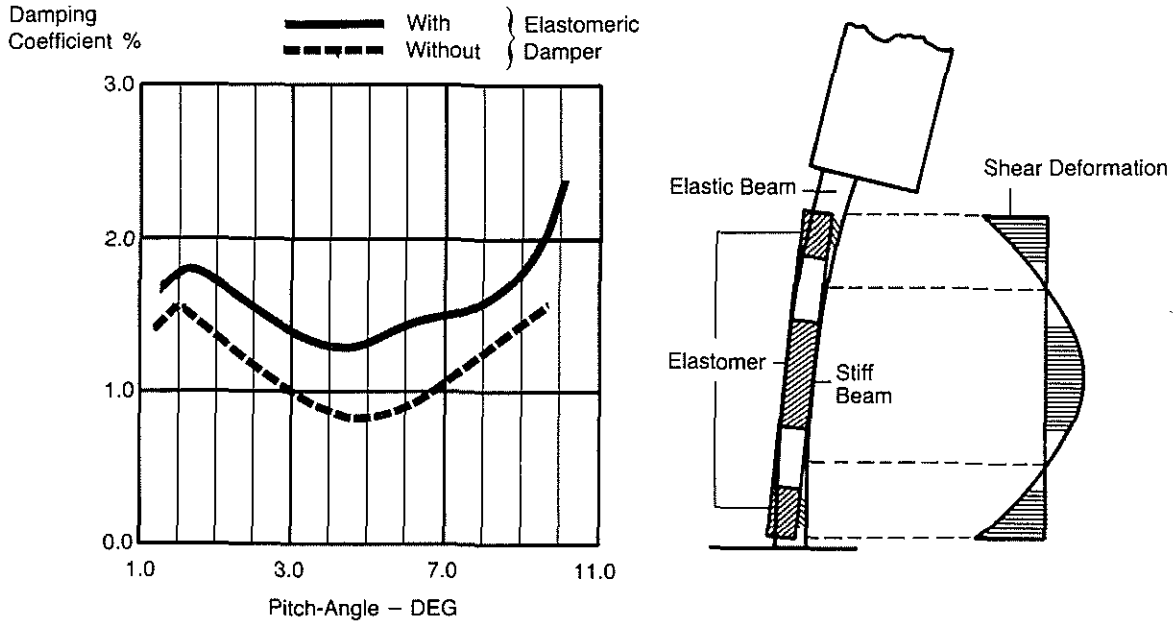

Figure 11 Influence of Elastomeric Damper - Principle and Whirl Tower Measurements

Owing to shear deformation of the elastomeric layer a part of the kinetic energy is dissipated. The measured blade damping of the rotor with and without damping element shows that 50% more modal damping can be expected. The absolute damping value is still relatively low. An influence of the damper on the natural frequencies could not be detected. The maximum strain measured during the whirl tests by simulating flight loads was about 6‰.

Consequences for Future Designs

The whirl tower tests and the component tests showed that the strains in the torsional elastic element owing to blade feathering can be increased Therefore in the final design the flexbeam could be about 25% shorter than in the experimental system. The tests also proved that it is sufficient to bond the elastomeric damper onto the flexbeam without any bolts. The tests confirm that the splice from the blade attachment to the flat flexbeam is well designed. This is an essential conclusion for a further reduction in the hub moment stiffness. Finally, the analytical calculations and models could be confirmed.

3.2 Advanced Bearingless Rotor Concepts

For the final rotor design two concepts have been pursued.

Rotor with Flexural Single Beam Element and Control Tube

Figure 12 shows the flexbeam element with cruciform cross-section.

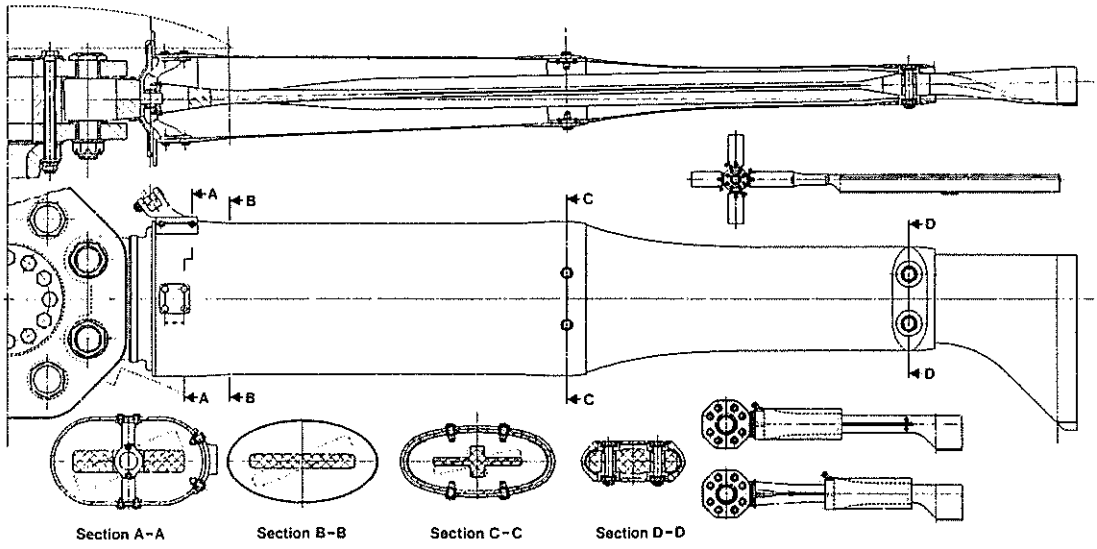

Figure 12 Composite Bearingless Main Rotor Design With Flexural Single Beam Element and Control Tube

The blade is controlled by an elliptic tube, which fairs the flexbeam element and the root of the blade. The tube is rigidly attached to the blade (section D-D) and is "fixed" inboard by a snubber, which transmits shear loads to the hub. For visual checking of the flexbeam, the tube can be telescoped. In order to reduce the hub moment stiffness the single beam element has inboard a structural "quasi-hinge" to accommodate blade flapping (section B-B).

Rotor with Flexural Double Beam Element and Control Rod

Figure 13 shows the double beam element with a T-type cross-section. This concept is similar to the Bearingless Main Rotor (BMR) of the Boeing Vertol Company (see Ref. 6). The flexbeam element consists of two separate parallel beams with a T-type cross-section. The blade is feathered by a control rod in the middle of the two flexbeams. The reduction of the hub moment stiffness is realized in the same way as for the single beam concept. A direct comparison of the two flexbeam designs is given in Figure 14. The outer part of the rotor blade is the same for both designs.

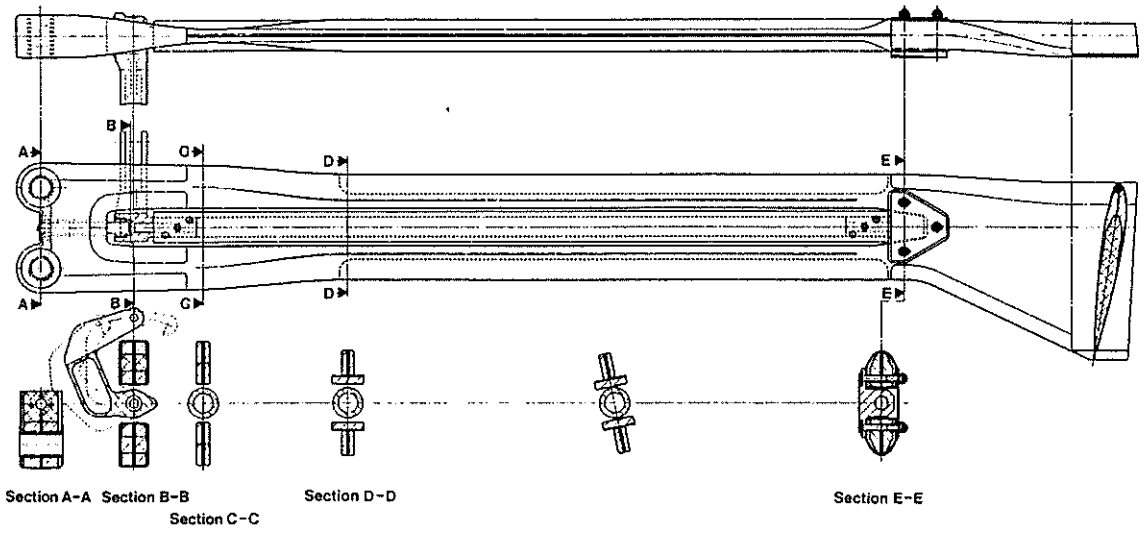

Figure 13 Composite Bearingless Main Rotor Design With Flexural Double Beam Element and Control Rod

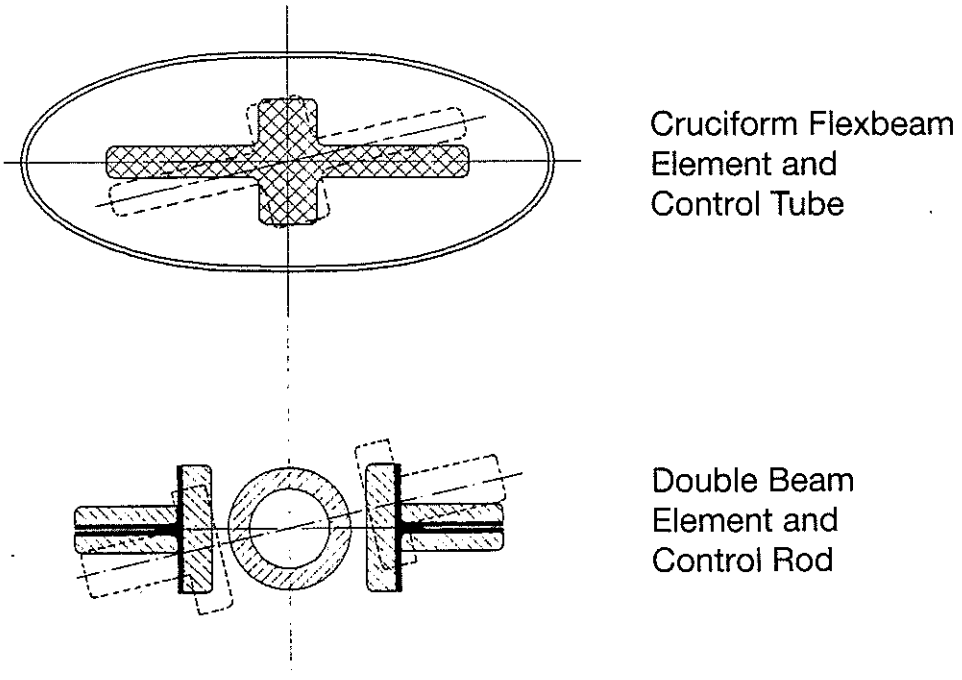

Figure 14 Cross-Section With Control Tube and Control Rod

Rotor Hub Design

Both bearingless rotor concepts are equipped with a new composite material rotor hub, see Figure 15. No precone angle is provided for the reasons of improving aeromechanical stability.

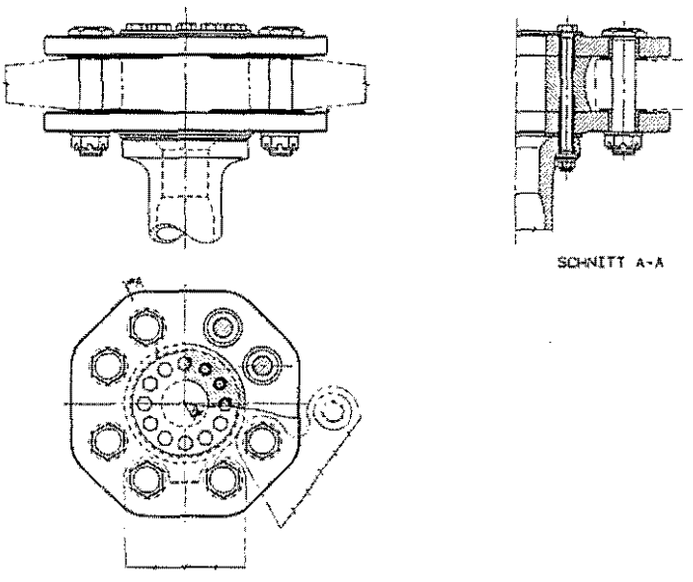

Figure 15 The Rotor Hub of Bearingless Main Rotor

The construction uses two flat plates made of quasiisotropic carbon fibre or glass fibre layers. These two plates are connected by a cylinder of carbon layers with a fibre orientation of 90° and $\pm 45^{\circ}$. The cylinder carries the pressure forces of the necked down bolts and the shear stresses. Figure 16 presents a finite element model of the hub which is used for the stiffness calculations.

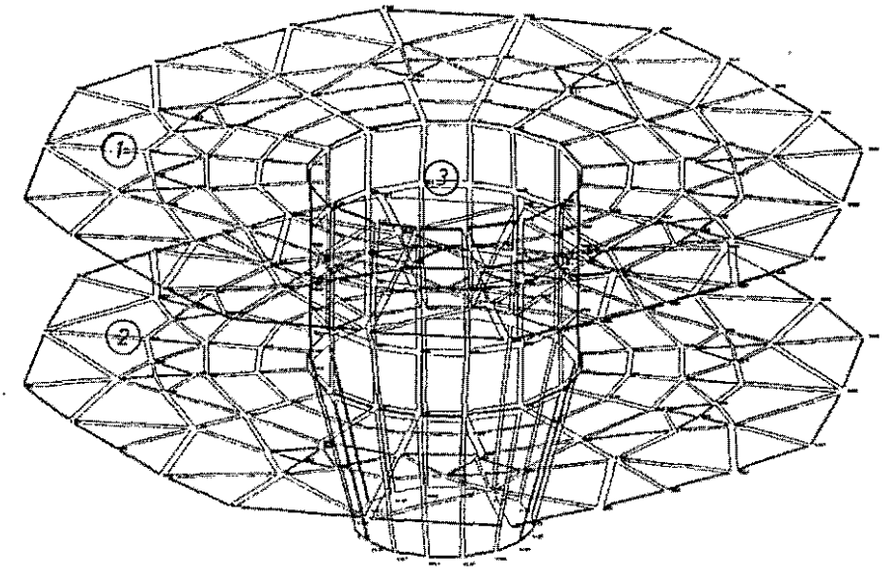

Figure 16 Finite Element Idealization of the Rotor Hub (Main Rotor)

Stiffness Tailoring

Theoretical investigations were carried out to harmonize the requirements for tuning the fundamental rotor blade bending and torsional frequencies and the ultimate strength conditions. Figure 17 shows the bending stiffnesses of the final design for the single flexbeam concept of Fig. 12 with blade feathering control by a tube.

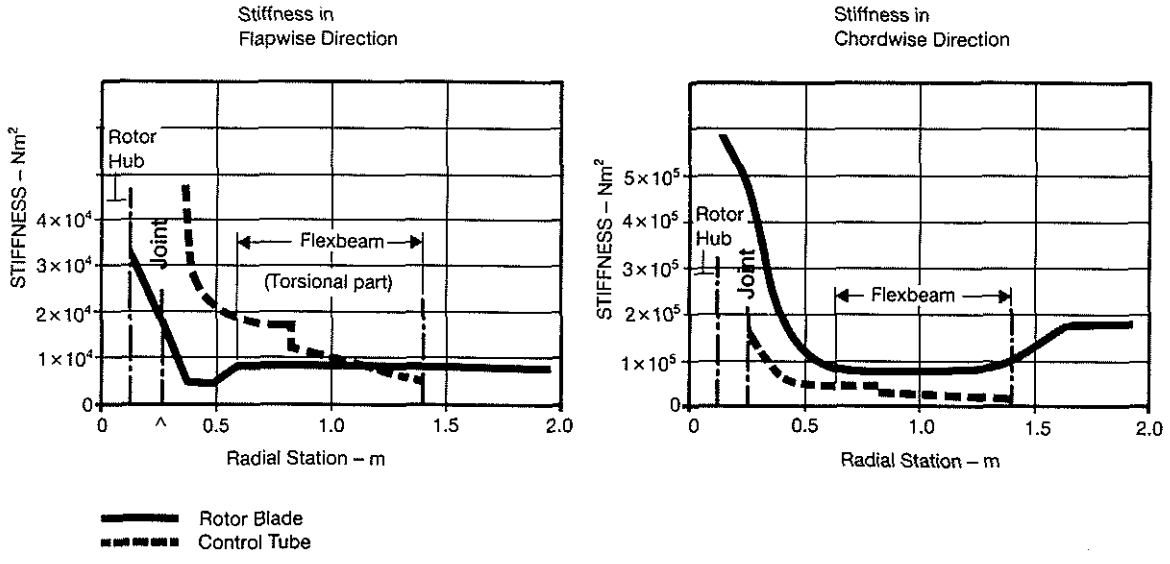

Figure 17 Bending Stiffness, Final Design of the Main Rotor.

The relative high stiffness of the control tube requires special attention in the structural dynamic analysis. The fundamental lead-lag bending mode is especially influenced by the tube. The calculated fundamental lead-lag frequency normalized by the rotor speed is 0.7. The influence of the torque tube on the fundamental flap bending frequency is minimized by placing the snubber near the "quasi-hinge", see Fig. 17 left. Thus a considerable reduction in the hub moment stiffness has been achieved. The virtual flapping hinge offset is 8.5% of the rotor radius. Some information about the 1/rev rotor blade and control tube bending moments in manoeuvre flight are given in Figure 18.

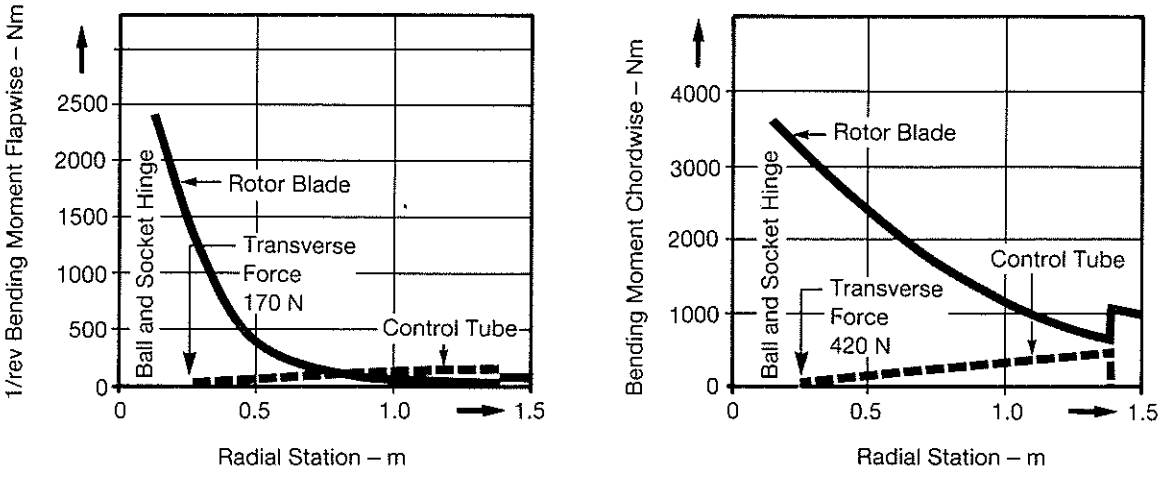

Figure 18 Estimated 1/rev Bending Moment (Amplitude) Distribution in Manoeuvre Flight at Max. Load Factor for the Bearingless Main Rotor

The stiffness tailoring of the double flexbeam concept brings about some new structural problems. Whereas the stiffness in the flapwise direction is similar to the concept with a single flexbeam, the stiffness characteristics in the chordwise direction are quite different. For the fundamental lead-lag bending mode the frame structure behaves like a single beam structure. For the second lead-lag bending mode however the effective stiffness is relatively low, because the double flexbeam element works as two separate beams. This structural dynamic behaviour has been confirmed by calculations and tests, see Figure 19. Further investigations were carried out and showed that some modifications of the rotor hub and blade attachment are necessary.

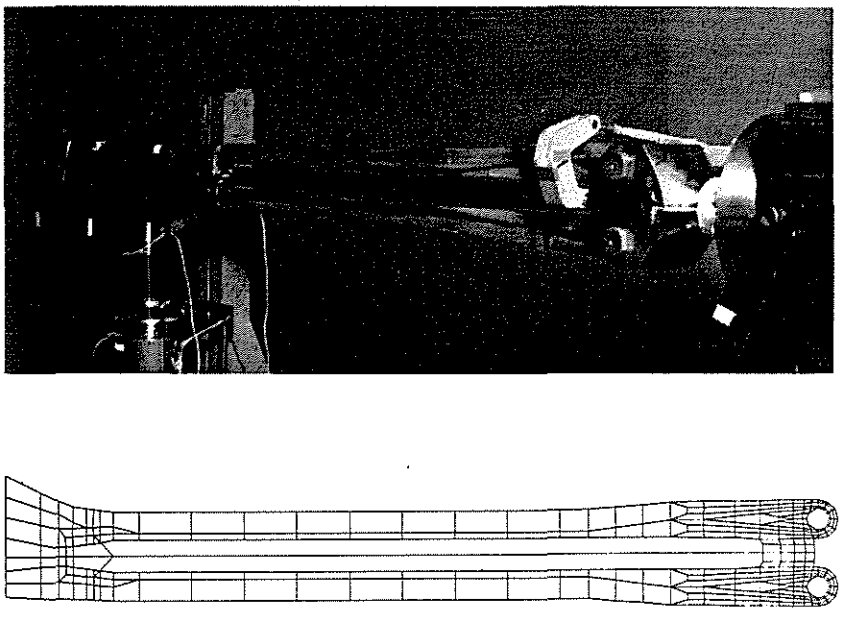

Figure 19 The Rotor Concept With the Double Flexbeam Test Setup and Finite Element Model

4. Development of the Bearingless Tail Rotor

A bearingless tail rotor for a light utility class helicopter is currently under development at MBB using a similar approach as for the main rotor. An experimental four-bladed soft-inplane rotor has been designed with BO 105 standard tail rotor blades for cost saving and availability. Meanwhile, the laboratory and whirl-tower tests with this rotor were performed with success. The rotor is now ready for flight testing on the BO 105/BK 117 helicopter. Further information about the tail rotor program is given in Ref. 7, 8.

4.1 Experimental Bearingless Tail Rotor Concept

Description of the Experimental Rotor

The basic principle of the construction is to build up the four-bladed system by two double-units. An overview of the rotor configuration mounted on the whirl-tower is given in Figure 20. The flexbeam element has a cruciform cross-section, see Fig.3. The canteliver pitch arm is fixed at the junction of the blade. This control configuration allows the introduction of pitch-flap coupling in a simple manner in order to reduce cyclic flapping in forward and maneouvre flight.

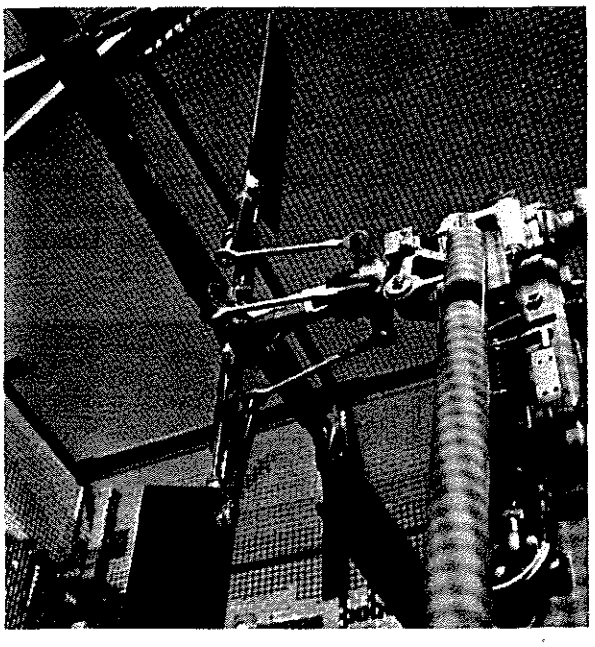

Figure 20 Collective Pitch Control of the Bearingless Tail Rotor (Experimental Version)

This soft-inplane bearingless tail rotor system has to be tailored carefully to avoid aeroelastic instability and response problems. Because of ground and air resonance stability considerations, the fundamental lead-lag bending frequency has been finally tuned at the relative high value of 0.77/rev. In addition, the structural lead-lag damping is augmented by an elastomer damping element which works in the same way as described for the main rotor

(see Fig. 11). The rotor blade flutter behaviour is strongly dependent on the torsional dynamics. Therefore the control system geometry and the bending stiffness of the pitch horn and flexbeam are of paramount influence. The geometry and the pitch arm/flexbeam configuration are presented in Figure 21 (without elastomeric damper). The pitch arm is designed in box-beam shape with carbon fibre composite unidirectional straps. This design guarantees a high bending stiffness at low mass.

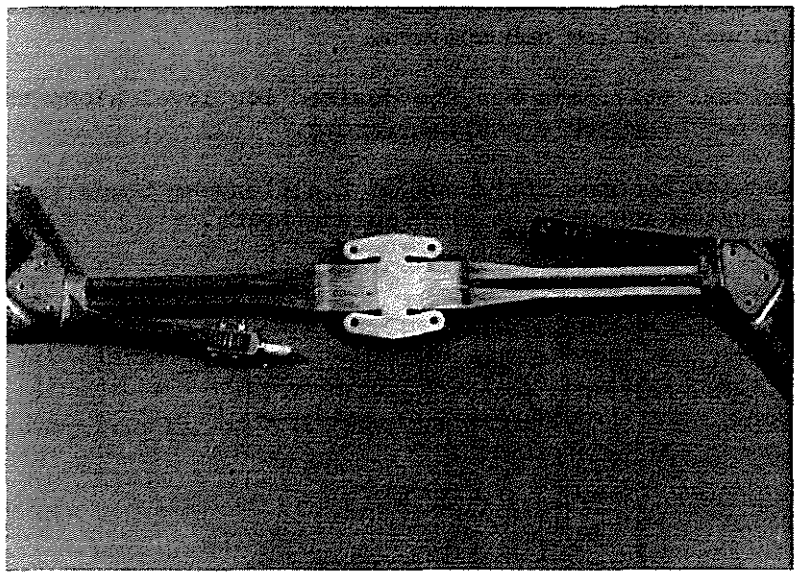

Figure 21 Torsional Elastic Element and Pitch Horn of the Tail Rotor (Experimental Version)

The centrifugal loads of opposite blades are carried within fibreglass straps from one blade to the other. The driving torque is transmitted to the rotor by four bolts which are placed beside the tension loaded rovings. In this way, the tension strain does not induce any force on the bolts. This mechanism was checked by a finite-element calculation whose results are plotted in Figure 22. The described principle of load introduction has the advantage that the region with the lowest flap stiffness can be shifted near the rotor axis.

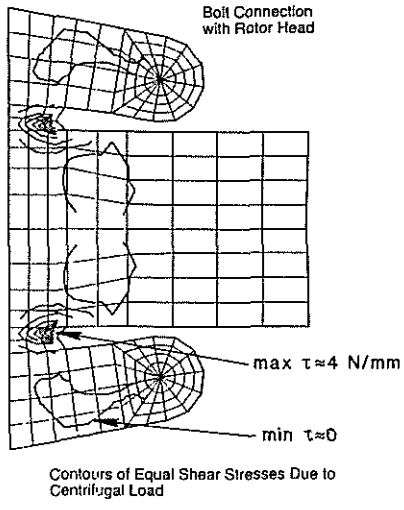

Contours of Equal Shear Stresses Due to Centrifugal Load

Figure 22 FEM Stress Calculation for the Tail Rotor Hub

Blade Stiffness Distribution

The radial bending and torsional stiffness distribution of the blade is plotted in Figure 23. The three stiffnesses are tailored carefully according to the various requirements of the bearingless tail rotor:

- The flapwise bending stiffness is greatly reduced inboard at a radial station of 2 to 6% of the rotor radius to produce a "quasi-hinge" for low hub moments.

- The torsional stiffness has the desired low level along the flexbeam for acceptable control forces.

- The chordwise bending stiffness of the flexbeam tunes the soft-inplane system and defines the inplane loads.

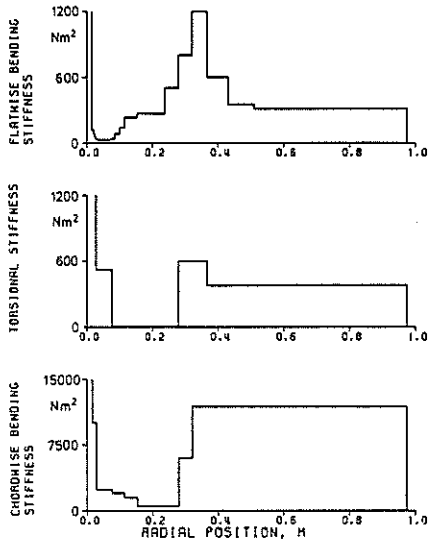

Figure 23 Stiffness Distribution of the Bearingless Tail Rotor (Experimental Version)

Blade Natural Frequencies

The blade frequencies are calculated at different rotor speeds with and without aerodynamics. The results are shown in Figure 24 and are in good agreement with available whirl test measurements. The first coupled flap-bending/torsion mode at zero and nominal rotor speed is illustrated in Figure 25. The pitch-flap coupling described by an effective δ_3-angle depends on the rotor speed and can be varied by the pitch arm length. The flutter stability is adversely influenced by a high positive δ_3-angle. The whirl-tower tests were performed with the "long" pitch arm configuration (effective $\delta_3 = 28^{\circ}$ at nominal rotor speed).

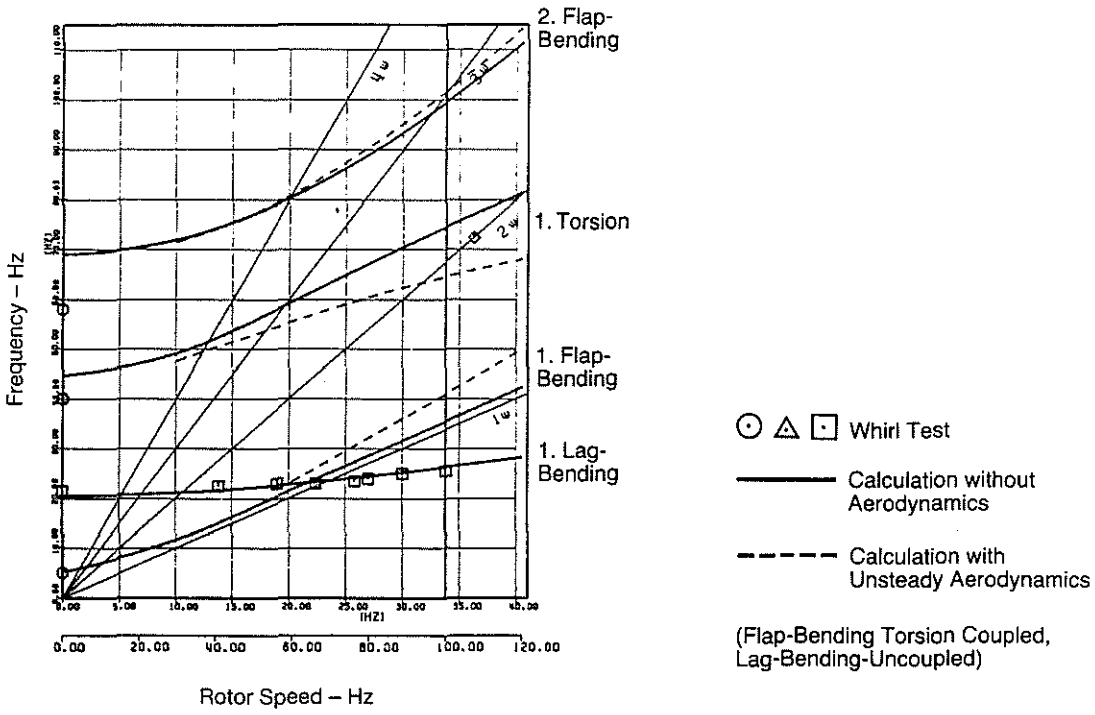

Figure 24 Experimental Tail Rotor Blade Natural Frequencies

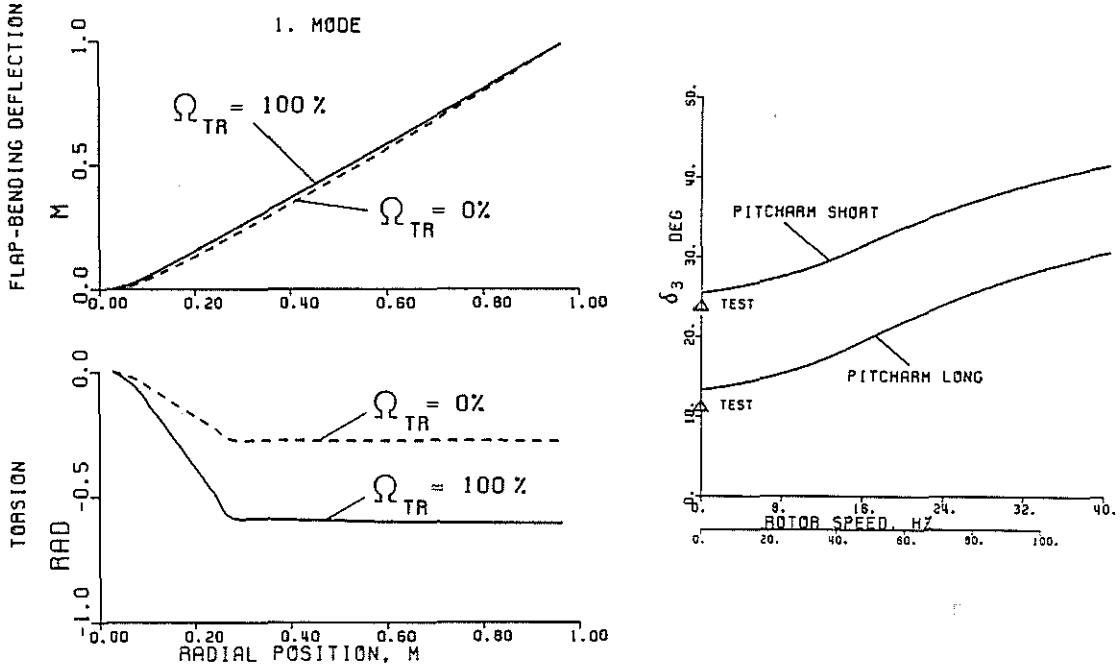

Figure 25 1. Coupled Bending-Torsion Mode Shape for the Bearingless Tail Rotor (Experimental Version)

Laboratory and Whirl-Tower Tests

The blade root and flexbeam element were fatigue tested for different loads, see Figure 26. In the following table the test loads and the load cycles are summarized.

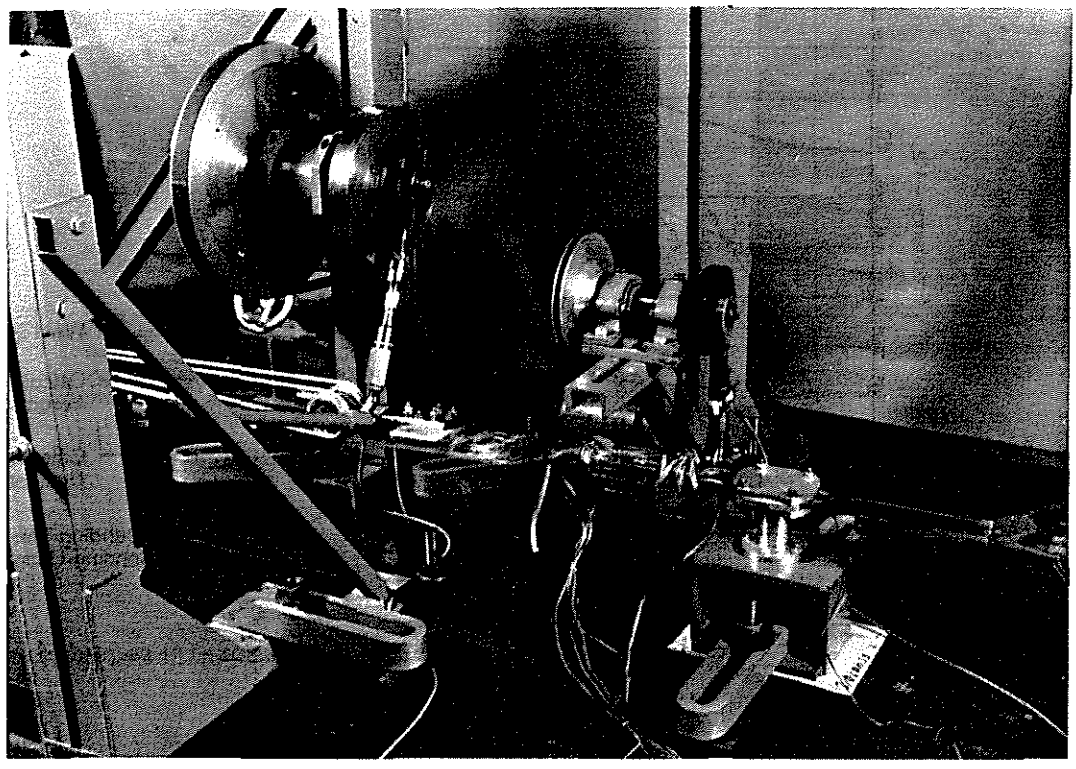

Figure 26 Test Setup for the Tail Rotor (Experimental Version)

Test Number	Load Cycles	Bending Moment [Nm]		Flexbeam Torsion-Moment [Nm]	Tension Load [kN]
		Flapwise direction	chordwise direction		
1	10^5	-	60 ± 50	-	-
2	10^6	-	± 140	-	-
	10^5	-	-	-	17 ± 15
3	10^7	combined load with		2.3 ± 1	27
	$2.5 \cdot 10^6$	max. strain of 10‰		2.3 ± 1	38

These test results confirmed the sophisticated design and its structural layout. In the subsequent whirl-tower tests the structural dynamics and aeroelastic characteristics were investigated. At maximum thrust, the highest strain of 8‰ corresponding to a stress of 320 N/mm^2 is measured at the "quasi-hinge". This result has been predicted by calculation, see Figure 27.

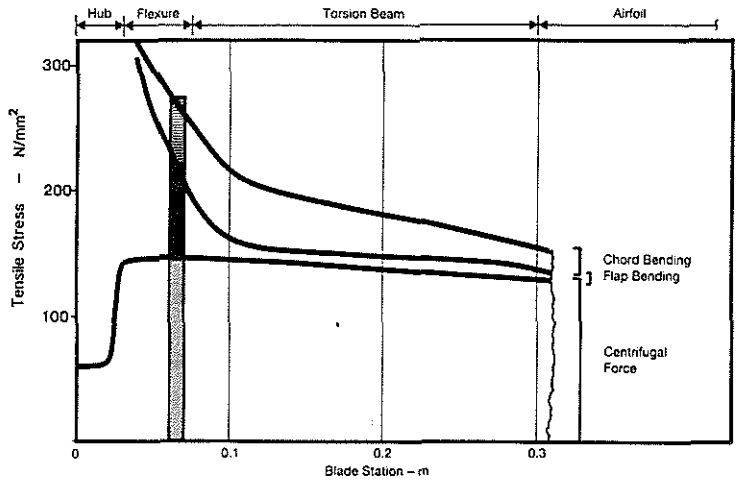

Figure 27 Predicted Tensile Stress Distribution of the Tail Rotor (Experimental Version)

The tensile stress consists of

50% due to centrifugal forces,

32% due to flap-bending moments,

and 18% due to lag-bending moments.

The measurements of the rotor blade natural frequencies (see Fig. 24) confirmed that,despite the relatively low fundamental torsional frequency of 2.1/rev, the rotor blade flutter margin was adequate within the rotor operation range. Lead-lag damping measurements showed that the pure structural damping of the fundamental mode is about 1.5% of the critical value. Thus the elastomeric damper has proved to be quite efficient.

4.2 Final Bearingless Tail Rotor Design

In further development, more advanced twisted blades with a reduced chord and lower mass will be used. The strains in the "quasi-hinge" can be reduced by these blades. In addition, the geometry and the composite material will also be redesigned for strain reduction. Mass balanced blades are provided for the final design for improving the aeroelastics.

5. Conclusions

The component and whirl-tower tests of MBB's soft-inplane bearingless main and tail rotors for light utility helicopters proved that this concept is practical. Both systems are ready for flight testing.

Modern composite material technology allows the tailoring of the torsional elastic flexbeam according to the various structural and dynamic requirements. Further efforts will be necessary in understanding the complex physics in order to make full use of the potential of the bearingless rotor concept. Simplicity, reliability and maintainability as well as the potential reduction of weight and costs have initiated the development of bearingless rotors. Even if these advantages are smaller than expected, the bearingless rotor opens greater new possibilities in the design of more comfortable helicopters, than are recognized today.

6. References

1) R.A.Ormiston: Investigations of Hingeless Rotor Stability
International Symposium on Aeroelasticity, Nuremberg, Oct.1981

2) H.Strehlow, B.Enenkl: Aeroelastic Design Consideration in the Development of Helicopters
56th AGARD Structures and Material Panel Meeting, London, April 1983

3) V. Klöppel, K.Kampa, B.Isselhorst: Aeromechanical Aspects in the Design of Hingeless/Bearingless Rotor Systems
9th European Rotorcraft Forum, Stresa, Sept. 1983

4) R.Wörndle:Calculations of the Cross Section Properties and the Shear Stresses of Composite Rotor Blades
7th European Rotorcraft and powered Lift Aircraft Forum, Garmisch-Partenkirchen, Sept. 1981

5) H.Huber: Gelenk- und lagerloser Hauptrotor in Faserverbundbauweise für dynamische Systeme zukünftiger Hubschrauber
3.BMFT-Statusseminar, Hamburg, Mai 1983

6) P.Dixon, H.Bishop: The Bearingless Main Rotor
Journal of the AHS, Vol.25, No.3, July 1980

7) H.Huber, H.Frommlet, W.Buchs: Development of a Bearingless Helicopter Tail Rotor
6th European Rotorcraft and Powered Lift Aircraft Forum, Bristol, Sept. 1980

8) H.Frommlet: Gelenk- und lagerloses Heckrotorsystem in Faserverbundbauweise
3. BMFT-Statusseminar, Hamburg, Mai 1983

7. Appendix: Summary of Rotor Data

	Main Rotor			Tail Rotor		
	BO105 Rotor	Experimental Rotor	Prototype	BO105 Rotor	Experimental Rotor	Prototype
Concept	Hingeless	Bearingless	Bearingless	See-Saw	Bearingless	Bearingless
Number of Blades	4	4	4	2	4	4
Radius	4.912 m	4.912 m	5.0 m	0.95 m	0.975 m	0.975 m
Rotor Speed	44.4 rad/s	44.4 rad/s	43.2 rad/s	227.2 rad/s	212.2 rad/s	212.2 rad/s
Blade Tip Speed	218.1 m/s	218.1 m/s	216.0 m/s	215.8 m/s	206.9 m/s	206.9 m/s
Cross Weight	2400 kg	-	2100 kg			
Max. Thrust				3100 N	3450 N	4800 N
Airfoil	NACA 23012	NACA 23012	DMH2/DMH1	NACA 0012	NACA 0012	S102 C-E
Blade Chord	0.27 m	0.27 m	0.3 m (0.2m at Blade Tip)	0.179 m	0.179 m	0.13 m
Twist	linear -10°	linear -10°	linear -10°	0	0	linear -10°
Blade Thickness	12 %	12 %	12% (9% at Blade Tip)	12 %	12 %	8.3 %
Relative Virtual Flapping Hinge Offset	14 %	12 %	8.5 %	0	5 %	5 %
Fundamental Lead-Lag Frequency	0.66/rev	0.68/rev	0.7/rev	1.8/rev	0.77/rev	0.7/rev
Fundamental Torsional Frequency	~ 3.7	~ 3.7	~ 4.4		2.1/rev	
Mass of Complete Rotor	211 kg	~ 225 kg	160 kg	8 kg	~7.3 kg	~7 kg